
Chapter 7

Ion Channels in Bursting Neurons

JAMES M. BOWER and DAVID BEEMAN

7.1 Introduction

The simple neuron model that we have built up over the past three chapters is what Llinás (1988) has referred to as the “Platonic Neuron”. In this idealized model, postsynaptic potentials in the dendrites (Chapter 6) propagate passively through the dendritic “cable” (Chapter 5) to the soma. Here, near the axon hillock, the summed and attenuated PSPs may activate voltage-dependent sodium and potassium channels that are very much like those found in the squid giant axon (Chapter 4). Although it was once assumed that this simplified description applied to most neurons, we now know that the situation can be much more complex.

In this chapter we are mainly concerned with the additional varieties of ionic conductances that are responsible for the wide variations in firing patterns seen in different neurons. Toward the end of the chapter, we examine a model that illustrates another difference between the Platonic neuron and many mammalian neurons. In many neurons, the dendrites are not merely passive conduits for the propagation of PSPs, but are endowed with a variety of conductances that can actively shape and amplify neuronal signals (Llinás 1988, Adams 1992).

In Chapter 4 we considered the ionic conductances underlying the generation of the action potential in the squid giant axon. This description of transmembrane sodium and potassium conductances constituted the first comprehensive and quantitative understanding of the ionic events associated with neuronal activity. As has often been the case in the

history of biology, this advance in understanding was dependent on the development and application of a new technology, the voltage clamp. However, equally important was the choice of the squid giant axon as the subject of the experiments.

This experimental preparation was chosen by Hodgkin and Huxley principally because the giant size of the squid's axon made the insertion of multiple electrodes possible. However, there is another reason that the choice of the squid axon was fortuitous. It turns out that the conductances found in this axon are fewer and more simplified than those found in any other region of a typical neuron. The reason is that axons, in general, are highly customized neural structures. In the squid, the giant axon is solely responsible for assuring the rapid and regular conduction of the neural impulse to the muscles of the squid's mantle. The repeated simultaneous contraction of these muscles, in turn, provides the force behind the animal's water-jet propulsion system.

Because the sole function of the squid giant axon is to conduct neural impulses in a rapid and highly regular fashion, the ionic conductances found in this axon's membrane are few and functionally streamlined. However, a very different situation holds for those neuronal regions, like the dendrite and cell body or soma, responsible for receiving and processing information and generating the patterns of activity distributed by the axon. Membranes in these regions often contain a much larger set of ionic conductances. Furthermore, the individual properties of these conductances are often customized to support the function a particular cell plays in the network in which it is found. As we show, these conductances can be quite rich and their interactions quite complex.

In general, the physiological behavior of a neuron, i.e., how it responds to input and generates output, is determined by the types of conductances found in its membranes and the interaction between them. In this chapter we specifically consider a set of ionic conductances that interact to produce periodic bursts of action potentials. The data presented are taken from experiments on the somata of periodically bursting molluscan neurons including those found in the sea slugs *Aplysia* and *Tritonia* as well as neurons in other related marine molluscs. As in the case of the squid giant axon, these cells have been extensively studied because their size and geometry made voltage clamp experiments considerably easier to carry out. Furthermore, individual cells are also readily identifiable from individual to individual allowing the experimenter to use multiple preparations to characterize each cell's properties (Frazier, Kandel, Kupfermann, Waziri and Coggeshall 1967). Although it was once believed that these varied molluscan ionic conductances were relevant only to the study of invertebrates, we now know that they are also found in mammalian neurons (Llinás 1988). Thus, single molluscan neurons can teach us much that is relevant to the understanding of the human brain (Kandel 1976).

As we shall see, different molluscan neurons make use of differences in the densities of these various types of channels to produce a wide variation in the shape and firing patterns of their action potentials. Variations in the voltage thresholds and time constants for activation and inactivation of these conductances are also used to produce differences in behavior. For

more complicated vertebrate neurons, variations in neuronal behavior are accomplished by differences in the distributions of these conductances over the soma and dendrites, not generally found in invertebrates.

We begin with a survey of the ionic conductances found in molluscan pacemaker neurons and a discussion of their effect upon the observed patterns of action potentials. Then, we make use of a GENESIS simulation of a particular bursting molluscan neuron in order to further understand the roles of these conductances. In the final section of this chapter, we use a GENESIS recreation of the Traub, Wong, Miles and Michelson (1991) hippocampal CA3 region pyramidal cell model, which has a similar set of conductances. With the tutorial simulation, we demonstrate how the burst firing of this mammalian neuron depends on the way that these conductances are distributed over the soma and dendrites.

7.2 General Properties of Molluscan Neurons

Individual molluscan neurons, like neurons everywhere, often have very different physiological properties. In any particular case, these properties are related to the information-processing role of the neuron within the animal. Neurons that are found in the abdominal ganglion of *Aplysia californica* are illustrative of the range of firing patterns that are found. Some cells have a stable resting potential and are silent in the absence of synaptic input. Others are never at rest and fire spontaneously. Those that discharge action potentials regularly and continuously at low frequencies, with a pattern like that shown for the *Aplysia* R3 neuron in Fig. 7.1A, are called *beaters*. *Regular bursters*, such as the R15 cell, generate a very regular pattern of bursts of action potentials, as shown in Fig. 7.1B. Still others, such as the L10 cell, generate irregular patterns of bursts, as shown in Fig. 7.1C.

In some cases, the periodic firing can be shown to be entirely endogenous to the neuron itself, and to persist even when the soma is isolated from the rest of the cell. These neurons have regular firing patterns in the absence of input and are often referred to as *pacemakers*. They are almost always associated with the control of behavior that is highly regular and subject to only moderate amounts of external regulation (e.g., respiration). In other neurons, varying amounts of not necessarily periodic input will generate a periodic neuronal output. These types of neurons are usually referred to as *conditional bursters* and tend to be associated with behaviors that are variably periodic but under considerable external control (e.g., swimming). Depending on modulation by synaptic input, they may be silent, beating, or bursting. The distinction between endogenous and conditional behavior is not always clear-cut. For example, the R15 neuron is usually called an *endogenous burster* because it fires spontaneously in the isolated soma, in the isolated ganglion, and in the isolated nervous system. However, recent experiments indicate that it is largely silent in the intact animal and might better be considered as a conditional burster (Alevizos, Weiss and Koester 1991).

The action potentials shown in Fig. 7.1 are produced primarily by channels that are

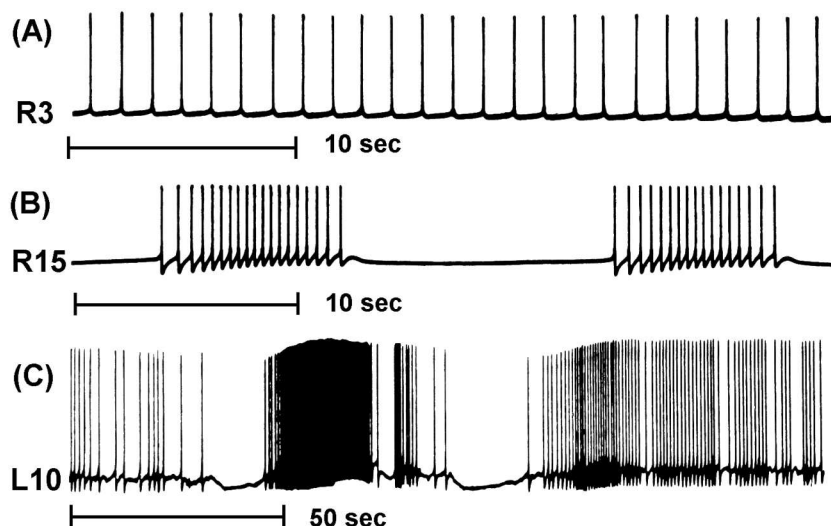


Figure 7.1 Some typical firing patterns of neurons found in the abdominal ganglion of *Aplysia*. (A) The R3 beater. (B) The R15 regular burster. (C) The irregularly bursting L10. (Adapted from *Cellular Basis of Behavior* (Kandel 1976). Copyright 1976 by W. H. Freeman and Sons. Used with permission.)

qualitatively similar to the sodium and potassium channels discussed in Chapter 4. As we shall see, the details of their shape and firing patterns are governed by other ionic conductances that are not present in the squid giant axon. Whether a particular neuron is a silent cell, beater, regular burster, conditional burster, or non-periodic is largely dependent on the particular combination of ionic conductances found in its cell membrane and on the interaction between them. Accordingly, understanding a cell's behavior is dependent on determining the types of conductances it contains, and the density of these conductances.

As mentioned in the previous section, the conductances found in parts of the neuron responsible for determining the overall input-output characteristics of the cell are considerably more complex than those found in its axon. This increased complexity is manifest in numerous ways. For example, these regions of a neuron often include conductances for ions other than sodium and potassium, including chloride and calcium. Second, the activation and inactivation properties of these conductances can be considerably more complex than those seen in the axon. In some cases, the activation and inactivation characteristics can not be adequately fit with the relatively simple exponential and sigmoidal functions used in the Hodgkin-Huxley model. In our model, this has necessitated the use of tabulated forms for some of the activation curves, rather than fits to an analytic function. Third, particular conductances can be voltage-dependent, dependent on the binding of particular molecules to the membrane, temperature-dependent, or a combination of all three. Fourth, the pharmacology of somatic ionic channels is often more complex, considerably compli-

cating experimental procedures. Nevertheless, as we show, a considerable amount is known about the ionic properties of molluscan neurons and the relationship of these properties to the function of individual cells. Finally, and most importantly, the temporal properties of specific conductances also vary considerably, with some having time constants in the millisecond range and others operating over minutes or even hours. These combinations of fast and slow time courses are responsible for the complex dynamics observed in bursting neurons.

7.3 Ionic Conductances — The Dance of the Ions

In this section we give a general overview of the principal ionic conductances that have been found in different molluscan neurons. As we demonstrate, different neurons contain different combinations of these conductances depending on the function they perform. Here, we describe a sodium conductance, a calcium conductance, a combined sodium-calcium conductance and three potassium conductances, one of which is dependent on calcium. Later, in Sec. 7.4.3, we give some details of the specific examples of these conductances that have been incorporated into our model molluscan burster. These conductances, listed on page 115 in Table 7.1, have been taken from various experimental measurements, and are representative of the conductances discussed in this section. Further details of these conductances may be found in the review article by Adams, Smith and Thompson (1980) and the many references given there. Although this is by no means a complete list of the conductances found in molluscan cells, considering the interactions between these primary conductances should provide some insight into how the overall behavior of a cell is influenced by the conductances its membrane contains.

Figure 7.2 presents steady-state activation and inactivation curves for each of the conductances used in the model. Chapter 4 has discussed the procedure by which these curves are obtained from voltage clamp experiments. In Part II of this book, Chapter 19 describes how one uses these experimental data to implement these channel models in GENESIS. In this chapter we consider the significance of their shape for cell function. In this regard it is important to note that the steepest changes in voltage dependence shown by the curves for any one conductance often tend to occur over a relatively narrow range of voltage. Furthermore, the values of steepest dependency vary for different conductances. As we will see, by comparing the region of largest change in activation and inactivation voltages with the observed action potentials, it is often possible to predict which aspect of neuronal signaling a particular conductance most influences. We will also see that the time constants for activation and inactivation of the various conductances have a great influence on the shape of the action potentials and the firing patterns. These have been listed in Table 7.1 near the nominal resting potential of the cell (-40 mV) and at a point during an action potential (0 mV). In this chapter, we use the variable X to represent the state variable for activation,

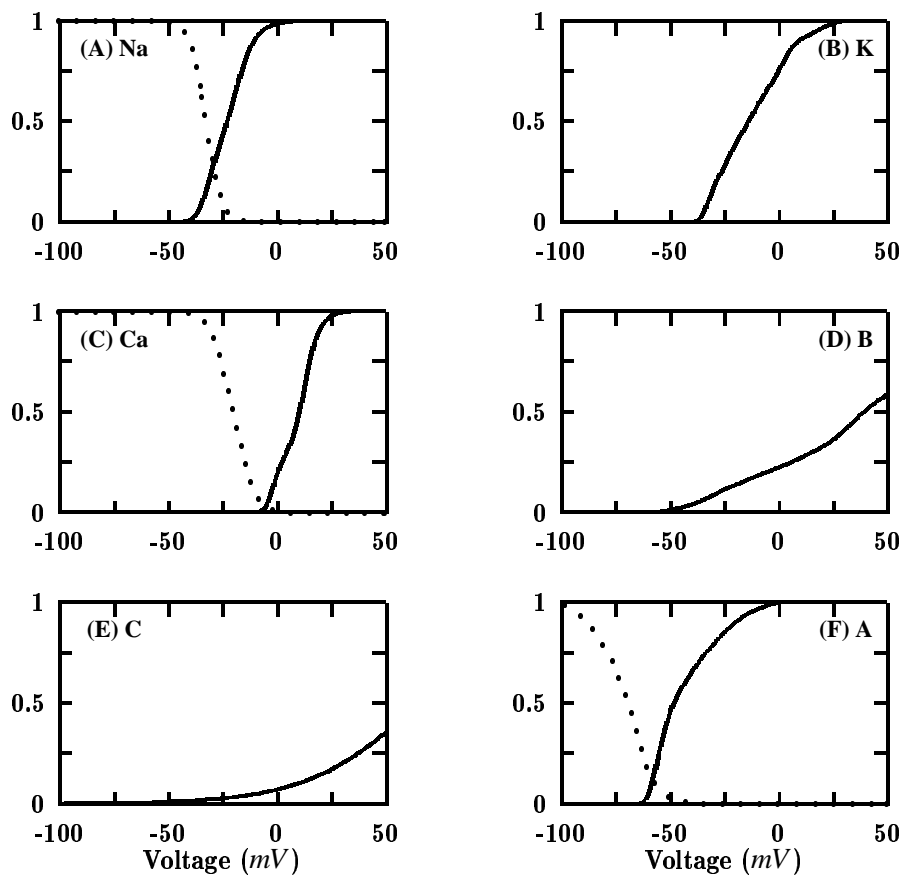


Figure 7.2 Steady-state activation variables (solid lines) and inactivation variables (dotted lines) for the conductances used in the bursting molluscan neuron model. (A) Fast sodium current. (B) Delayed potassium current. (C) High threshold calcium current. (D) Slow inward “B-current.” (E) Calcium-dependent potassium “C-current,” with $[Ca^{2+}]$ held at 187 nM . (F) Transient potassium “A-current.”

and Y to represent the state variable for inactivation. In the case of the squid axon sodium channel, these would correspond to the variables m and h , used in Chapter 4.

7.3.1 Action Potential Related Conductances

The first three conductances to be considered in this section are all involved directly in the voltage changes associated with the action potential. As we will see, action potentials generated in molluscan somata are dependent on sodium and potassium associated ionic

conductances that are similar, although not identical, to those described in the squid axon by Hodgkin and Huxley. In addition, however, many molluscan neurons also include an action potential related calcium conductance. Although not seen in the main body of the squid axon, this conductance is similar in many ways to one found in its terminal region (Llinás, Steinberg and Walton 1976).

Fast Sodium Conductance

The somata of action potential generating molluscan neurons include a rapidly activating sodium conductance. As can be seen in Fig. 7.2A, the region of largest voltage-dependent change in this channel's activity is at and above the threshold for generation of the action potential. Thus, in the molluscan soma, as in the squid axon, this conductance is associated with the generation of the action potential. In both soma and axon this sodium conductance is also generally described by X^pY^q kinetics and is usually blocked by TTX, suggesting that the conductances are homologous.

Although the axonal and somatic sodium conductances are similar, there are important physiological and pharmacological differences between the two indicating that the channels on which they are based are not identical. One of the differences between these conductances is that a prolonged period of hyperpolarization does not inactivate the somatic conductance as it does in the axon. The result is that many molluscan somata do not generate the “anode break” phenomena briefly discussed in Chapter 4. In Exercise 5, you have an opportunity to discover what features of the activation and inactivation kinetics account for this difference. In addition, the exponent associated with the activation term X can vary in molluscan somata. In fact, differences in activation kinetics are often seen between different molluscan neurons of the same species, resulting in faster action potential rise times in one neuron compared to another. Similarly, the actual voltage dependencies of the activation and inactivation curves can vary from cell to cell. This variation tends to be correlated with differences in the normal resting membrane potential of a particular neuron, with shifts in the positive direction in cells with higher resting potentials and vice versa. In this way, this classic sodium conductance is often customized to the characteristics of a particular neuron.

Delayed Potassium Conductance

In addition to the sodium conductance, the potassium conductance of the squid axon also has a homologue in the molluscan soma. Evaluating the activation curve for this conductance (Fig. 7.2B) suggests that this somatic conductance is also associated with the action potential's falling voltage phase. Thus, as in the squid axon, this potassium conductance is also responsible for repolarizing the membrane after sodium influx. Table 7.1 shows that, as with the squid axon, the time constant for activation of the potassium current is much larger than that for the sodium current. For this reason, it is often referred to as the *delayed*

or *late* potassium current. As the channel conductance is much greater with depolarizing voltages than with hyperpolarizing voltages, it is also called the *delayed rectifier* current.

However, as with the sodium conductance, this potassium conductance also differs from the axonal version in several ways. We may see some of these differences by comparing the steady-state activation curve for this current in a typical mollusc (Fig. 7.2B), with that in the squid axon (Fig. 4.9). Whereas the potassium activation increases sigmoidally, beginning at voltages below the resting potential in the squid axon, the molluscan activation curve starts much more abruptly, beginning at a point above the action potential threshold. Table 7.1 shows that the exponent for the activation parameter is also different, with the conductance being proportional to X^2 for the molluscan potassium current, instead of X^4 .

Another important variation concerns the presence of a voltage-dependent inactivation, which has been observed in the dorid molluscs *Anisidoris* and *Archidoris* (Connor and Stevens 1971a, Aldrich, Getting and Thompson 1979a). This inactivation is more complex than that modeled by Hodgkin and Huxley for the sodium conductance, as the recovery from inactivation is at least an order of magnitude slower than the onset. This effect is often referred to as frequency-dependent inactivation because, as a neuron fires repetitively, the baseline inactivation of the potassium conductance increases. The buildup of inactivation occurs with a relatively long time constant and is slowly reversed when the neuron stops firing. Some decline in potassium current has also been observed in *Aplysia* during long periods of depolarization. However, it has been suggested that in *Aplysia*, the effect is largely due to the accumulation of potassium in the extracellular solution at the membrane surface, reducing the potassium equilibrium potential (Adams and Gage 1979a).

High Threshold Calcium Conductance

One of the ways in which the region of the squid axon studied by Hodgkin and Huxley is particularly unusual as neural tissue is in the complete absence of a calcium conductance. However, the contribution of the squid to membrane biophysics has not been limited to use of its giant axon. In addition, the giant synapse that activates the giant axon has also been used to quantify the properties of a particularly important and ubiquitous calcium conductance (Llinás et al. 1976). This conductance is activated by the occurrence of an action potential and results in the influx of calcium that directly triggers transmitter release.

Because calcium has not been considered before in these chapters, and because it occupies a special place in cell function, we briefly consider the special role played by this ion and the experimental consequences. Calcium conductances, in general, are an important property of the membranes of not only most neurons but also of a wide range of other living cells. The influx or intracellular release of calcium is used quite universally as a trigger for important cellular functions. Cell cleavage during development is triggered by calcium. Calcium is also involved in many fundamental cellular properties through its role in regulating numerous metabolic enzymes.

Beyond its general effects on cell physiology, calcium also plays a host of important specific roles in neurons. Perhaps one of the best known involves the calcium triggered release of neurotransmitter from the presynaptic axon terminal (Katz and Miledi 1969). This calcium conductance underlies the neural machinery involved in transferring information from one cell to another. Of more relevance to this discussion, calcium conductances are also found in the somata and dendrites of many different types of neurons. In some cases these conductances are quite small, whereas in others, membrane voltage changes associated with calcium entry can rival sodium in its responsibility for generating action potentials.

Although calcium is an exceedingly important contributor to neuronal function, it is also typically very difficult to study. In the axon terminal, for example, the minute size of the calcium conductance makes its isolation very difficult even with voltage clamp techniques. In other cases calcium conductances can have long and complex time courses. In addition, the study of pure calcium entry is usually confounded by potassium conductances that are quite difficult to completely block and can largely mask calcium ion flow. Finally, the very close relationship between intracellular calcium and many fundamental metabolic pathways makes it difficult to perform calcium ion substitutions, which are an important experimental approach to isolating the ions associated with different membrane conductances. Ion channel biophysicists must often be at their most clever and careful when studying calcium.

Here, we examine one of the several calcium conductances that are known to exist in molluscan somata. Although its kinetics are much slower, the *high threshold* calcium conductance is qualitatively similar to the sodium conductance in that it inactivates with a time constant that is much greater than that for its activation. Looking at the voltage-dependent activation and inactivation curves for the *Aplysia* R15 calcium conductance (Fig. 7.1C), it can be seen that the steepest region of its voltage dependence is associated with peak voltage values in the action potential. As a result, these calcium channels are maximally activated during and immediately following the action potential's peak voltage, and are not activated in the absence of action potentials. Because of the delay in activation, the calcium channels are maximally activated during the action potential's negative going phase. Because the equilibrium potential for calcium is very positive, this means that there is a tremendous driving force for calcium entry into the cell. Voltage clamp data in the giant synapse also suggest that calcium entry occurs during the falling phase of the action potential. It turns out that this high threshold action potential associated calcium conductance has a homologue in many neurons, including mammalian as well as molluscan neurons (Linás 1988).

Although the threshold for activation of this conductance is generally above that for the activation of the sodium conductance, there is a large variation in the threshold among different classes of molluscan neurons. For example, it begins to activate at potentials as low as -40 mV in the dorid molluscs (Aldrich, Getting and Thompson 1979b). The physiological effect of this lower threshold appears as a "shoulder" on the downward slope of the action potentials in these neurons. This effect is examined in Exercise 6. Neurons

in dorid molluscs that have this shoulder in the action potential also show a progressive frequency-dependent broadening of the action potentials. This arises as a result of an interaction between the calcium conductance and the frequency-dependent inactivation of the potassium conductance, also observed in these neurons. The longer period of depolarization provided by the shoulder allows the potassium conductance to inactivate, further increasing the width of the shoulder with each successive action potential.

7.3.2 Control of Bursting Properties

The trace of a typical R15 bursting pattern shown in Fig. 7.1B reveals some interesting features which we would like to explain from the properties of ionic conductances that are found in this cell. Typically, bursts are characterized by groups of 2–20 spikes, separated by long (5–30 second) postburst hyperpolarizations. During a burst, the spike frequency first increases and then decreases, and for some cells a plot of the interspike interval as a function of time is approximately parabolic (Strumwasser 1965). There is a slow depolarizing bump after the last spike in a burst, and the bursts appear to be riding on a slow wave of depolarization. In fact, when the sodium conductance is blocked with the neurotoxin TTX and the action potentials cease, slow oscillations are seen that have a period approximately equal to that of the bursts (Strumwasser 1968). Wilson and Wachtel (1974) conducted voltage clamp experiments on a variety of bursting neurons in *Aplysia*. When the steady-state total channel current is plotted as a function of clamping voltage (using the inward negative convention), the resulting curve shows a *negative slope region* (NSR). They proposed that this negative resistance characteristic is essential for the existence of the slow oscillation and burst firing.

It turns out that regulation of the bursting properties of these cells involves additional conductances that control how, when, and for how long neurons are active. In general, control of input-output relationships of individual neurons is largely associated with potassium conductances. The result is that the diversity of neuronal activity patterns is directly paralleled by the diversity and complexity of intrinsic potassium conductances. In the final part of this section we consider two of these conductances.

There are several different mechanisms and conductances that can lead to this sort of oscillation in the firing. In general, we require an inward current with a long time constant in order to produce the sustained depolarization that initiates and maintains the burst. We need another mechanism to terminate the burst and provide a long, but finite, period of hyperpolarization between the bursts. As these two processes involve time scales that are much slower than those for the action potential related conductances described earlier, they may be studied in isolation from these faster conductances by observing the slow *tail currents* that are seen in voltage clamp experiments after the initial rapid changes in current (Smith and Thompson 1987). On the other hand, the slow currents are generally much smaller in magnitude, and are also difficult to separate from each other. For this reason,

there is a great deal of uncertainty as to the ionic basis of these currents and in the measured activation curves.

The slow inward current discussed below is often called the “B-current,” or “burst current.” The basis of the slow hyperpolarizing current has been particularly controversial. Several researchers have concluded that it is a potassium current which becomes activated by the buildup of intracellular Ca^{2+} ions during the burst (Gorman, Hermann and Thomas 1982, Smith and Thompson 1987). This current is often called the “C-current.” At some point, the C-current polarizes the cell below the threshold for the production of action potentials and the burst terminates. During the hyperpolarized interval after the burst, no calcium ions enter the cell and the Ca^{2+} concentration begins to slowly decay, reducing the C-current. The cell then slowly depolarizes, activating the B-current and leading to a new burst of action potentials.

However, other researchers have found that the slow hyperpolarizing current is insensitive to the external K^+ concentration and does not reverse at the expected potassium equilibrium potential (Adams and Levitan 1985, Kramer and Zucker 1985b). They concluded that it cannot be a potassium current and attributed it to the inactivation of an inward calcium current. It turns out that both mechanisms are present, but that the C-current dominates at low temperatures (10–15 °C). At higher temperatures, the C-current is still present, but decays much more rapidly than the potassium-insensitive current (Thompson, Smith and Johnson 1986). It is often the case that, when nature can find two ways to accomplish the same purpose, both methods are used. The *Aplysia* must function in a variety of environments ranging from the cold ocean floor to warm tidepools, so the two different currents provide a way to maintain burst production over a wide temperature range. As the inactivation of the slow inward current has not been as thoroughly investigated or quantified as the calcium-activated potassium current, we concentrate on the currents that dominate at low temperatures in the rest of this section and in our model. A description of the hypothesized currents and bursting mechanisms at room temperature may be found in the review article by Benson and Adams (1989).

Finally, we should briefly mention another mechanism for burst production that is found in some mammalian neurons. The transient low threshold calcium current, or T-current, is found in neurons in many parts of the mammalian nervous system, including the thalamus, inferior olive, superior colliculus, and medial septum, as well as other regions of the brainstem and forebrain. This current is qualitatively similar to the high threshold calcium current discussed in Sec. 7.3.1, but has a much lower threshold for activation and inactivation. Consequently, a small depolarization from a hyperpolarized level can activate the T-current, producing a broad hump that is above the threshold for generating sodium spikes. After activation, it inactivates and cannot be reactivated until the cell is hyperpolarized again. The result is that a burst of action potentials is generated which rides upon the hump (McCormick 1990, McCormick, Huguenard and Strowbridge 1992). For larger depolarizations from the resting potential, the T-current is completely inactivated. In this

case, the cell will either be silent, or if the depolarization is large enough, tonically fire trains of single spikes. In thalamic relay neurons, these different modes of firing are used to gate the sleep-wakefulness cycle. During drowsiness and slow wave sleep, the cells are hyperpolarized and fire in bursts. This results in synchronized cortical oscillations which may be observed in electroencephalograms. Increased excitatory synaptic input from the brainstem and hypothalamus occurs during periods of wakefulness, switching the neurons into the single spike firing mode. In this case, the cells serve as relay elements carrying information to and from the cortex (Llinás 1988, McCormick et al. 1992). Chapter 17 provides the information that will allow you to create your own simulation of a thalamic relay cell.

In the final section of this chapter, we examine yet another mechanism for generation of bursts in mammalian neurons. Currents that are very similar to those found in molluscan bursters produce burst firing in hippocampal CA3 region pyramidal cells. However, in this case, the mechanism for burst production depends upon the structure of the cell and the fact that there are different densities of the various conductances in the soma and dendrites.

Bursting Conductance

Molluscan neurons that burst endogenously often have a specific burst-related conductance. When one of the action potentials from such a neuron is observed in isolation, it can be seen that the action potential is followed by a large depolarization. This can be clearly seen after the final spike in one of the bursts shown in Fig. 7.1B. This depolarizing after-potential is associated with the B-current described here. This slow inward current activates over a period of about one second.

The B-current is difficult to measure because of its small amplitude and because its time course is similar to the decay of the outward C-current. It has been variously attributed to a current of sodium ions (Barker and Smith 1978), calcium ions (Gorman et al. 1982), or a combination of the two (Smith and Thompson 1987). In bursting *Tritonia* neurons, the amplitude of this current is reduced by about 50% when the extracellular solution is replaced by one having one tenth the normal concentration of Na^+ ions. A similar result occurs when the Ca^{2+} concentration is reduced instead. When both ions are absent, the current vanishes. This suggests that in these neurons, Na^+ and Ca^{2+} ions make approximately equal contributions to the B-current (Smith and Thompson 1987). It is also possible that this current arises from two separate ion-specific conductances that have similar time and voltage dependencies. Kramer and Zucker (1985a) found that in *Aplysia* bursting pacemakers L2 through L6, the slow inward current is activated by intracellular calcium. However, these experiments in *Tritonia* showed a voltage dependence that is inconsistent with activation by calcium. Thus, it is possible that the mechanism of activation of the current and the ionic selectivity may be different in the various molluscan bursting pacemaker neurons which have been studied.

Figure 7.2D shows the voltage dependence of the channel activation, taken from measurements of the B-current in bursting *Tritonia* neurons by Smith and Thompson (1987). It can be seen that the B-current begins to be activated in this cell at about -50 mV , well below the point at which the fast sodium conductance is activated. The activation continues to increase throughout the rising phase of the action potential. Taking into account the delay in the conductance onset, it is not surprising that the physiological effect of this conductance is to produce a post-action potential depolarization of the cell soma. Although the total conductance of this channel is about 1% of that associated with the sodium channel, because it is active throughout the voltage range of the action potential and is also active when the cell membrane is at relatively high resistances, this conductance can produce large transmembrane voltage effects.

As mentioned before, the principal physiological effect of this conductance is to depolarize the neuron after the action potential. In fact, this post action potential depolarization alone is often sufficient to produce a second action potential in the cell. Accordingly, once the cell is depolarized, this conductance makes the pacemaker capable of generating repetitive firing with little or no additional input. Furthermore, Table 7.1 shows that the time constant for activation of this conductance is much smaller during an action potential (240 msec at 0 mV) than it is at more polarized levels (1.2 sec at -40 mV). Thus, the B-current increases comparatively rapidly during an action potential, but decays slowly between action potentials, becoming progressively larger with each action potential. Combined with the action potential related conductances discussed in the previous section, this should result in patterns of continuous firing. However, as is clear from Fig. 7.1B, these intrinsically driven bursting patterns eventually terminate. Next, we consider one of the mechanisms responsible for the termination of the burst.

Calcium-Activated Potassium Conductance

In addition to the slow inward current described above, voltage clamp experiments on bursting neurons in *Aplysia* and *Tritonia* show an outward tail current that slowly decays over many seconds after repolarization from a depolarizing voltage step (Thompson et al. 1986, Smith and Thompson 1987). At cold temperatures ($10\text{--}15\text{ }^\circ\text{C}$), the amplitude of this current depends strongly upon the extracellular concentration of K^+ ions. When the K^+ concentration of the extracellular solution is increased in order to shift the potassium reversal potential to the clamping voltage, the current may be eliminated entirely, indicating that it is a potassium current. By performing voltage clamp experiments at a variety of extracellular K^+ concentrations, it is possible to separate this current from the B-current, which is insensitive to the external K^+ concentration (Smith and Thompson 1987).

The apparent voltage dependence of the activation of this current is unusual in that it is bell-shaped, rising to a peak at about $+40\text{ mV}$ and then decreasing with further depolarization. The explanation for the observed activation properties has to do with the fact that this

conductance is calcium-dependent. Although the channel associated with this conductance is selectively permeable to potassium, channel opening appears to require the presence of intracellular free calcium. The associated current is often called the C-current. As the cell is depolarized, calcium ions enter via the B-current, activating the C-current. However, as the clamping voltage increases towards the calcium reversal potential, the inward flow of Ca^{2+} decreases, causing a drop in the activation. The calcium dependence of this conductance may be verified by experiments that prevent the intracellular concentration of Ca^{2+} from increasing during depolarization. For example, the substitution of Co^{2+} , a Ca^{2+} current blocker, for Ca^{2+} in the external solution suppresses the C-current (Smith and Thompson 1987).

Gorman and Thomas (1980) performed voltage clamp experiments on *Aplysia* R15 neurons in which Ca^{2+} ions were directly injected into the soma through micro-electrodes. The resulting concentration of free intracellular Ca^{2+} was determined from changes in the absorbance of light by the Ca^{2+} sensitive dye arsenazo III. These experiments revealed that the C-current varies linearly with internal Ca^{2+} over a wide range of concentrations. The intrinsic voltage dependence of the activation of this conductance was observed by using Ca^{2+} injection to hold the internal Ca^{2+} concentration constant. This resulted in the exponential voltage dependence seen in Fig. 7.2E. A comparison of this activation curve with that of the late potassium conductance shown in Fig. 7.2B reveals some significant differences between the two conductances. Rather than having a rapid rise in activation after a fairly sharp threshold for activation, the activation curve for the C-current increases gradually with voltage, with no clear threshold for activation. This suggests that the two conductances may arise from distinct populations of ion channels.

The very slow variation in the C-current after depolarizations or action potentials contributes to spike frequency adaption as well as the long period of postburst hyperpolarization. Both of these have a powerful effect upon the integrative function of the neuron. Because this current, which is also prevalent throughout the mammalian nervous system, depends strongly on the internal Ca^{2+} concentration, it has the potential to be modified by factors that affect cellular metabolism, such as hormones or synaptic modulators (Adams et al. 1980).

Transient Potassium Conductance

Finally, we consider one additional potassium conductance that also influences the action potential generating properties of molluscan as well as many other species of neurons. The associated current is known as the A-current and is found throughout the nervous system. In addition to being kinetically separable from the delayed rectifier, the A-current is also pharmacologically distinct. It is interesting to note that this conductance is actually as ubiquitous as the delayed rectifier in neurons. In fact, the principal reason that it is not as well known as the other potassium conductance is that it does not occur in the squid axon. It has

been suggested that this conductance is actually the phylogenetically oldest conductance and that it is the precursor for the sodium channel (Hille 1984). This conductance has also been isolated to a single gene locus in the fruitfly, *Drosophila*. The *shaker* mutation of this gene prevents the A-current from inactivating, resulting in the prolongation of action potentials and causing the fly to shake violently when it is anesthetized.

Table 7.1 reveals that unlike the delayed potassium current, which inactivates very slowly or not at all, the A-current inactivates moderately rapidly (235 msec) after a fast (12 msec) activation. Thus, its response to a depolarizing pulse is a short-lived outward flow of current. For this reason, it is often called the “transient outward current”.

Figure 7.2E displays the voltage dependencies of activation and inactivation of this conductance and illustrates another significant difference from the conductances that we have considered so far. Unlike the previously described conductances, its steepest voltage dependencies are found in a voltage range near or below resting membrane values. This fits with the role of this conductance in regulating the threshold behavior of the neuron. At the resting potential for the neuron the activation curve for this conductance is quite steep and the time constant for activation is very short. Because the equilibrium potential for potassium is near the resting potential of most neurons, the effect of this conductance is to resist any rapid depolarization of the neuron. As a consequence, transient inputs do not result in the generation of action potentials. However, a sustained input above the resting potential causes the A-current to inactivate, allowing the cell to be driven to the threshold for firing. Note that it is the delayed potassium current, however, which is responsible for the repolarization that follows an action potential. This is because it is strongly activated (with a delay) during the peak of the action potential. At these high potentials, the A-current is completely inactivated and makes no contribution until the cell has become hyperpolarized.

The low thresholds for activation and inactivation of the A-current are responsible for another important function of this conductance. During the hyperpolarization following a spike, the potential is such that the steady-state activation of the delayed potassium current would be zero, so it is decaying with a time constant of about 60 msec. When the A-current is present, it will be activated at these hyperpolarized potentials. Thus, it will produce an outward current that maintains the hyperpolarization, slowing the onset of the next action potential. This allows the cell to produce the slow firing that is typical of pacemaker cells. With increasing input to the cell (and higher membrane potentials), the value of the inactivation parameter for the A-current decreases, so it is less effective in prolonging the hyperpolarization. Thus, it gives the cell the ability to perform a “frequency encoding,” transforming the membrane potential level to spike frequency. This is evident during the bursts shown in Fig. 7.1B. As the B-current grows and increases the average after-spike membrane potential, the firing rate increases. Toward the end of the burst, as the C-current begins to dominate and hyperpolarize the cell, the firing slows. Exercise 4 provides an opportunity to examine this behavior in detail.

7.4 A Model Molluscan Neuron

The cell that is modeled is a “generic burster,” loosely modeled after the *Aplysia* R15 cell at temperatures below 16°C, although it contains channel models taken from measurements on bursting neurons in *Tritonia* and *Anisidoris* as well. Thus, the simulation is presented as an exercise in modeling and a study of the various conductances discussed in the previous section, not as an accurate model of a specific neuron. By implementing the model within the *Neurokit* cell building environment, we have made it possible to modify nearly all of the relevant parameters of the model and its channels while running the simulation. As we have mentioned, the abundant varieties of molluscan pacemaker neurons have numerous features in common. For example, we will see in Exercise 2 that by simply modifying the relative proportions of the six channel types which we have described, we can convert the model from a burster to a beater.

There are some other recent models of the R15 cell that include the channels that dominate the bursting behavior at higher temperatures (Canavier, Clark and Byrne 1991, Canavier, Baxter, Clark and Byrne 1993, Bertram 1993). Butera, Clark, Canavier, Baxter and Byrne (1995) have produced a very detailed model containing 12 state variables and over 50 parameters. More recently, this has been used as the basis for a simplified four-variable model that exhibits many of the characteristics of the activity of the more detailed model (Butera, Clark and Byrne, 1996). After studying Part II of this book, you may wish to use the information given in Chapter 19 to implement one of these models, or to modify the model given here to include these channels.

7.4.1 Adrift in Parameter Space

When choosing the default parameters for a complex model, it would be best if we could obtain all the needed information directly from experimental data, with no adjustable parameters. Unfortunately, this is rarely, if ever, possible.

Chapter 11 discusses some general issues and approaches to guide you in the construction of realistic neural models. In the case of single cell models, the usual approach is to first determine an anatomically correct compartmental representation of the cell and to determine its passive membrane properties. The second step is to incorporate active channels into the model, based on experimental evidence for their existence. As much as possible, the channels should be modeled using the best available experimental data for conductance densities and activation variables. Often, the most complete data come from experiments on different types of neurons in different species, and performed at different temperatures. Also, measurements often show that, even for different examples of the same identifiable cell in the same species, there are large variations of conductance densities and the voltage dependence of channel state parameters.

This uncertainty in the model parameters means that constructing a model neuron usu-

ally involves a third step of searching *parameter space*, in order to find a consistent set of model parameters that will enable the model neuron to duplicate the experimentally observed behavior of the actual cell. This may be quite time consuming, as there may be many parameters that could be relevant to the model's behavior, and there may be large uncertainties in their values. When the channel kinetics are obtained from other neurons than the one being modeled, one can make a first pass at refining the channel parameters by some translation and scaling of the state variables. For example, the voltage dependence of activation curves may be shifted to take into account different resting potentials, or the time constants may be scaled to take temperature differences into account. However, it is often necessary to make a systematic search over parameter space, varying the channel densities and kinetics in order to fit published physiological responses of the cell. The differential equations that describe such a model have a very large number of parameters which could be varied. Although these equations must be solved numerically, there are a number of methods of mathematical analysis that can narrow down the search.

When modeling bursting neurons, it is possible to make use of the vastly different time scales for the spiking and the burst cycle behaviors in order to divide the problem into separate fast and slow subsystems. This can simplify the process of choosing parameters that are consistent with both kinds of behaviors (Rinzel and Lee 1987). Phase plane analysis (Rinzel and Ermentrout 1989) is another useful tool. Instead of plotting one variable as a function of time, one time-dependent variable is plotted as a function of another. For example, the activation variable for the slow hyperpolarizing current may be plotted against calcium concentration, or the membrane potential may be plotted against calcium concentration. Analysis of these plots then suggests ranges of parameters that lead to slow wave oscillations and bursting behavior, and those that lead to beating behavior (Rinzel and Lee 1987, Canavier et al. 1991, 1993). The requirement that plots of the steady-state total channel current as a function of clamp voltage should have a region of negative slope (the NSR) can be used to adjust the maximum conductance for the slow hyperpolarizing current (Bertram 1993).

The next release of GENESIS (likely to be available by the time you read this) will contain a library of routines that may be used to perform automated searches over large regions of parameter space. These may be used to fit the model parameters that govern firing characteristics to the results of current clamp or other experiments (Bhalla and Bower 1993, Vanier and Bower 1996). The parameter search methods implemented in this library include simulated annealing, genetic algorithms, conjugate gradient, stochastic search and simple brute-force search. These are often used to run many versions of a simulation in parallel on a parallel computer, or over a network of workstations (see Sec. 21.7).

For the simple structure of our molluscan neuron, the first step in modeling was relatively straightforward. We have largely neglected the final stage of "fine tuning" our model parameters, leaving this for those readers who are interested in doing so. Instead, we have concentrated on the second stage, and have used the best experimental data that we have

for the channel activations and conductance densities, making changes only as they were required. In our discussion of the implementation of the model, we give the reasons for some of the choices that were made when adjusting parameters. This may give you some guidance when constructing your own models or varying the parameters of this model. The decisions that were made in modeling the hippocampal CA3 pyramidal cell (Sec. 7.6) are described in some detail in the paper by Traub et al. (1991).

7.4.2 Implementation of the Model

One of the first computer simulations of the ionic currents and the resulting action potentials in giant molluscan neurons was performed by Connor and Stevens (1971c), who modeled beating pacemaker neurons in the molluscs *Anisidoris* and *Archidoris*. Like bursting neurons in *Aplysia*, these typically have a single axo-dendritic process extending from a large spherical soma that has a diameter of 250–300 μm . In most of the voltage clamp experiments upon which the channel models were based, the soma was isolated from the rest of the cell. As we are interested in the endogenous firing properties of the neuron, and not in the details of synaptic input, we can model the cell as Connor and Stevens did, treating it as a single soma compartment that contains the voltage-activated channels.

In our simulation, it is convenient to model this with a cylindrical compartment that has both a length and a diameter of 250 μm , and thus has the same surface area as a sphere with a 250 μm diameter. The membrane potential of this compartment will then obey an equation similar to Eq. 2.1, or to the combination of Eqs. 4.1 and 4.3 which describe the behavior of a section of the squid giant axon. As we will have additional channels, we can write it in the form

$$C_m \frac{dV_m}{dt} = \frac{(E_{rest} - V_m)}{R_m} + \sum_k I_k + I_{inject}, \quad (7.1)$$

where the sum over k represents a sum over the different types of ionic currents I_k that are present.

As in Chapter 5, the membrane resistance R_m (in ohms) and capacitance C_m (in farads) are related to the surface area of the cell A and the specific resistance and capacitance by $R_m = R_M/A$ and $C_m = AC_M$. In the model, we have used the Connor and Stevens values of the specific membrane resistance, $R_M = 4.0 \Omega \cdot \text{m}^2$ ($g_{leak} = 0.25 \text{ S}/\text{m}^2$), and the specific capacitance, $C_M = 0.07 \text{ F}/\text{m}^2$. Likewise, we have used their value for the nominal resting potential of the cell, $E_{rest} = -40 \text{ mV}$. Although an endogenous burster is never “at rest,” this potential is close to the threshold at which action potentials begin in the R15 and other molluscan bursters. The value of the specific membrane capacitance, which is close to the value measured for the *Aplysia* soma (Adams and Gage 1979a), is much larger than the nearly universal value of $0.01 \text{ F}/\text{m}^2$ found for most cell membranes. It is likely that this large value arises because the highly infolded membrane of the molluscan soma has a much

Current	p	q	E_{rev} (mV)	\bar{g} (S/m ³)	τ_X (msec)		τ_Y (msec)	
					-40 mV	0 mV	-40 mV	0 mV
Na	3	1	50	138	12	1.6	50	17
K	2	0	-68	66	61	31	—	—
Ca	2	1	64	65	4	5.4	100	177
B	1	0	68	5	1200	240	—	—
C	1	0	-68	124	3800	3800	—	—
A	4	1	68	82	12	12	235	235

Table 7.1 Exponents for activation (p) and inactivation (q), reversal potentials (E_{rev}), conductance densities (\bar{g}) and time constants (τ_X and τ_Y) for the ion channels used in the molluscan burster model. For a given channel type, the conductance per unit membrane area is $\bar{g}X^pY^q$.

larger surface area than that calculated by assuming a smooth spherical surface, as we have done here (Coggeshall 1967). All of these parameters, as well as the soma dimensions, may be varied in the simulation.

For each conductance in the model, we write the ionic current in the form

$$I_k = A\bar{g}X^pY^q(E_{rev} - V_m), \quad (7.2)$$

where A is the area of the soma, \bar{g} is the conductance density (maximum channel conductance per unit area), E_{rev} is the reversal potential for the ion, and the variables X and Y represent its activation and inactivation state variables.

Note that I_k appears on the right hand side of Eq. 7.1. This, along with the sign of $(E_{rev} - V_m)$ in Eq. 7.2, indicates that we are using the convention that a current of positive ions *into* the cell is to be considered to be a positive current, rather than the “physiologists’ convention” introduced in Chapter 4. We will use this sign convention throughout this chapter and in plotting currents in the two tutorial simulations. For each of the ion currents used in the model, Table 7.1 summarizes the values of the channel conductance densities \bar{g} , the reversal potentials E_{rev} , and the exponents p and q for activation and inactivation. It also gives the time constants for activation and inactivation (τ_X and τ_Y) at E_{rest} (-40 mV) and at a voltage during an action potential (0 mV).

7.4.3 Modeling the Channels

The six types of channel conductances were modeled following the procedures described in Chapter 19. This involved fitting the voltage dependencies of the steady-state activation and inactivation parameters and their time constants to data taken from published results of voltage clamp experiments on molluscan pacemaker neurons. Except as noted, the channel conductance densities given in Table 7.1 have been estimated from these experimental data. In the model, we have used more significant figures than are justified for most of the

conductance densities. We will leave it as an exercise for you to vary their values and to determine which parameters, if any, may be sensitive to changes on the order of 10% or more.

Action Potential Related Conductances

The data for the fast sodium conductance were taken from measurements on the *Aplysia* R15 cell by Adams and Gage (1979b). However, the activation curve X was shifted downward by -5 mV, making it more like that for the fast inward current conductance quantified by Connor and Stevens (1971b). This produced more robust firing when used with the other conductances in the model.

The delayed potassium conductance parameters were fitted to data taken by Thompson (1977) from bursting LPL2 and LPL3 cells in *Tritonia*. However, the potassium reversal potential was taken to be that measured in *Aplysia* by Adams and Gage. Inactivation of this current was not included in the model.

The high threshold calcium conductance was modeled from *Aplysia* R15 cell measurements by Adams and Gage (1979b). The measured reversal potential shown in Table 7.1 is lower than that for most mammalian neurons. This is due to the relatively high concentration of Ca^{2+} ions inside the cell of molluscan neurons (Adams and Gage 1979a).

Burst Related Conductances

The bursting conductance (B-current) was modeled from data taken from bursting cells RPL2, LPL2 and LPL3 in *Tritonia* (Smith and Thompson 1987). However, the current due to this conductance was treated as a pure Ca^{2+} current, rather than that from a combination of Ca^{2+} and Na^+ . This is probably more like the situation in *Aplysia* (Gorman et al. 1982). In order to provide sufficient depolarizing drive to maintain the burst for several seconds, it was necessary to increase the conductance density to a value several times greater than that found in the *Tritonia* measurements. Smith and Thompson noted that the amplitude of I_B in different preparations was quite variable, more so than any other current measured. It was largest in cells that were bursting most strongly. Note from Table 7.1 that this conductance is nevertheless far smaller than that for any of the other conductances. The reversal potential (64 mV) is close to that for the calcium current, as would be expected. However, it was difficult to measure, and was determined only within the very large experimental uncertainty of ± 59 mV. You may wish to explore the effect of increasing the value E_{rev} and decreasing the value of \bar{g} when experimenting with the simulation.

The steady-state activation for the calcium-activated potassium conductance (Fig. 7.2E) was fitted to the previously discussed *Aplysia* R15 measurements of Gorman and Thomas (1980) when the internal Ca^{2+} concentration was held constant at approximately 187 nM. The value for the conductance density ($\bar{g} = 124$ S/m³) was estimated from the Gorman

and Thomas results, and used with no further adjustments. As the activation was found to depend linearly on the Ca^{2+} concentration, we can determine the channel current at any other concentration by scaling Eq. 7.2 by the factor $[\text{Ca}^{2+}]/187$, where $[\text{Ca}^{2+}]$ is the internal Ca^{2+} concentration in nM . Thus, we need to model the way that Ca^{2+} varies with time and membrane potential. In addition, it is necessary to estimate the time constant for the intrinsic voltage dependence of the channel activation, independent from time variations in $[\text{Ca}^{2+}]$.

Chapter 19 describes how the variation of $[\text{Ca}^{2+}]$ may be modeled by an equation of the form

$$\frac{d[\text{Ca}^{2+}]}{dt} = BI_{Ca} - \frac{[\text{Ca}^{2+}]}{\tau}. \quad (7.3)$$

The first term on the right gives the rate of increase of $[\text{Ca}^{2+}]$ due to an inward channel current I_{Ca} . In this model, the current is the sum of the B-current and the high threshold calcium current. As discussed in Sec. 19.4.1, it is difficult to calculate the constant of proportionality B from first principles. A value of 1000 moles/ampere/ m^3 was chosen in order to give reasonable bursting behavior and increases of $[\text{Ca}^{2+}]$ that are typical of those measured during a burst. The second term represents an attempt to fit the various processes that deplete $[\text{Ca}^{2+}]$ to an exponential decay with a single time constant, τ . Gorman and Thomas found τ to be 17.5 sec from their Ca^{2+} injection experiments.

The remaining question is to determine the time constant for activation of the voltage-dependent conductance for a fixed $[\text{Ca}^{2+}]$. Gorman and Thomas estimated that for a depolarizing step from -50 mV to 110 mV, the time constant for activation is only 12 msec. However, this is far outside of the region of interest for our simulation, as we are particularly interested in the rate of decay of the hyperpolarized phase between bursts. It is also fairly common for activation time constants to be much larger at low voltages than at higher voltages. Thus, we have estimated the time constants from measurements made by Thompson et al. (1986). They found that when *Aplysia* L2 cells were repolarized to -40 mV after a depolarizing step, the C-current decayed exponentially with a time constant of about 3.1 sec. As this includes the effect of the decay of $[\text{Ca}^{2+}]$, we estimated the activation time constant τ_X from the relation $1/\tau_X + 1/\tau = 1/\tau_{net}$, obtaining the value of 3.8 sec listed in Table 7.1. For convenience, it was assumed to be constant over the range of interest.

The transient potassium conductance model was taken from the Connor and Stevens (1971c) measurements of the A-current activation and inactivation state variables in beating *Anisidoris* pacemaker neurons. These are very similar to those found by Thompson (1977) for bursting *Tritonia* neurons. For consistency with the other potassium conductances used in the model, a reversal potential of -68 mV was used, rather than the slightly higher value measured in *Anisidoris*.

7.5 The Molluscan Neuron Simulation

The model that we have described in the previous section has been incorporated into a simulation based upon the *Neurokit* cell builder environment. This tutorial then provides an introduction to *Neurokit*, as well as an opportunity to further explore the roles that these six conductances play in determining neural behavior. *Neurokit* is an elaborate GENESIS simulation that can create a cell model from a file which describes the morphology of the cell and the channels which it contains. Once a cell has been loaded into *Neurokit*, you will be able to modify it extensively and perform a variety of experiments. This means that you will be able to use the same simulation and menu system to study the properties of both the molluscan burster and the more complex CA3 pyramidal cell model.

Neurokit may be used with multi-compartmental models to change the geometry and electrical characteristics of compartments, and to add, delete, and reposition them within the neuron. It also allows channels to be deleted from compartments and for new channels to be added from one of the GENESIS libraries of predefined channels. Its channel editing facilities may be used to modify activation curves and their time constants. Thus, it is possible to construct and modify sophisticated single neuron models with little or no GENESIS programming.

In this tutorial, we explain and use only a few of the basic features of *Neurokit*. The experiment described here and the exercises at the end of the chapter should help you to learn more about the ways that the six basic channel types of this model can affect its firing patterns. If you wish to learn more about the advanced features of *Neurokit*, you may run it from the *Scripts/neurokit* directory and try some of the examples that are suggested in the on-line help. (Alternatively, you may print out the *README* file.) In Part II of this book, Chapter 17 describes how you may use *Neurokit* to implement your own cell models.

7.5.1 Using Neurokit

In order to allow room for the graphical display, move a terminal window into the lower left-hand corner of your screen. (This is normally done by using the left mouse button to click and drag on the title bar of the window.) After changing into the directory in which the simulation resides (usually *Scripts/burster*), type “genesis *Neurokit*” to the UNIX prompt. Chapter 17 explains the details of the initialization files that are used by *Neurokit* to load a particular cell model. There will be a delay while the simulation is being set up, and eventually, a title bar with the options

```
quit  help  file  run cell  edit cell  edit compt  edit channel
```

will appear at the top of the screen. Click on the `help` button, and a brief summary of the model and instructions for running the simulation will be displayed. When you feel that

you are ready to begin, click on the `CANCEL` button at the bottom of the help window. The next time that you call up `help`, you will return to the same place in the help file.

Click on the `file` option on the title bar. The `file` menu will appear, showing various dialog boxes which indicate that we are running the `mollusc` cell model simulation. As the default values in the boxes are all correct, click the `Load from file` button on the `file` menu. A few obscure messages will appear in your terminal window. Then click `run cell` on the title bar. You should see the `SIMULATION CONTROL PANEL` and two “Cell Windows,” each containing a representation of the cell with a graph below. The graphs have been initialized to plot the membrane potential at the left and the internal concentration of calcium ions at the right. (In our SI units, 10^{-6} moles/ m^3 = 1 *nM* concentration.) In other experiments, we may use the `scale` button in the upper left corner of the second Cell Window to plot other quantities of interest, such as the current, conductance, or activation variable for a given channel.

Initially, the `Recording` button under the `ELECTROPHYSIOLOGY` heading will be highlighted, indicating that you are ready to plant recording electrodes in the cell. Start by clicking the left mouse button in the round soma in each Cell Window. A recording electrode should appear in each cell and the boxes labeled `click_site1` and `click_site2` should each display “/`mollusc/soma`,” Other buttons under the `ELECTROPHYSIOLOGY` heading provide options for performing current clamp and voltage clamp experiments and for applying various types of synaptic input to models that contain synaptically activated channels.

We would like to begin by examining the endogenous bursting of this model in the absence of any input, so go ahead and click on `run` in the `SIMULATION CONTROL PANEL`. The dialog box for `runtime` indicates that the simulation will run for 40 seconds of simulated time each time you click on `run`. The `refresh_factor` dialog indicates that the graph will be updated every five time steps. This gives a reasonable compromise between execution speed and accuracy in depicting the details of the action potentials, but you will notice that the action potentials will have irregular heights. If you need to examine individual action potentials in detail and don’t mind the slower performance, you may wish to set this value to “1” and decrease the time step in the `clock` dialog box. If you wish to examine a burst in more detail, or to run the simulation for a longer period of time, click on the `scale` button in a graph window to bring up a menu for changing the scales used for the plots.

7.5.2 Understanding the Results

Once the run has finished, let’s try to understand what we see in the two plots. The simulation begins with all channel conductances initialized to their steady-state values when the membrane potential is clamped to the nominal resting potential of -40 *mV*. Of course, this cell is never “at rest,” so the initial burst of spikes will be slightly different from the following ones. After the end of the first burst of action potentials, there is a gradual decrease in V_m , reaching a maximum hyperpolarization of about -58 *mV*. The membrane potential

then begins to increase. Once it gets over about -50 mV, the rate of increase accelerates. Once it gets near -40 mV, the cell begins firing again. At this point, the calcium concentration is at its minimum value. During the burst of action potentials, the concentration rises rapidly, reaching its maximum at the end of the burst. It then begins a slow decline during the interburst interval.

We can understand this behavior by looking at the activation variables and their time constants. The activation variables are plotted in Fig. 7.2, and Table 7.1 shows the corresponding time constants at membrane potentials of -40 mV and 0 mV. However, *Neurokit* allows us to both edit and view the voltage dependence of the steady-state activation variables, their time constants, and the corresponding Hodgkin-Huxley rate constants α and β (Eqs. 4.21 and 4.22). This may be done by clicking on `edit channel` in the title bar. This will bring up a Cell Window at the lower left containing the green spherical soma. Click on the soma. It will turn red, and icons representing the soma and the six channel types will appear in the Compartment Window at the upper right. Begin by clicking on the icon for the B-current in order to select it. The `gate` dialog box will show the default gate to be examined, the X gate. Position the cursor in this box and hit "Return." The resulting plots will reveal that the slow inward B-current begins activating at about -50 mV, with a time constant of about 2 seconds. (The graph for steady-state activation or inactivation curve plots is labeled `m_inf` to correspond to the symbol m_∞ often used for the Na activation gate.) This should explain the basis for the buildup of the depolarization that allows action potentials to be generated during the burst. Also examine the activation and inactivation (Y gate) for the Ca current. When is it likely to make a significant contribution to the Ca^{2+} concentration? Examine the activation of the C-current. In the simulation menus and icons, we represent this type of conductance by the symbol `K_C`, in order to distinguish it from the faster potassium conductance `K` which is associated with action potentials. The outward current due to this channel will be proportional to its activation, the internal Ca^{2+} concentration, and the difference between the membrane potential and the Ca reversal potential. Can you use this to understand how the burst is terminated and how the hyperpolarized interval comes to an end? Later, you may wish to experiment with the effects of applying offsets (`ox` and `oy` dialogs) or scaling (`sx` and `sy`) of the activation curves or their time constants. This procedure is described in Exercise 6 and is discussed in more detail later in Part II, Sec. 19.2.2.

It may also be helpful to examine the various channel currents over the course of the simulation. We could use the second Cell Window to plot one of the channel currents instead of the Ca^{2+} concentration, but there is another way that will let us see all six channel currents at the same time. The `run paradigm` button in the SIMULATION CONTROL PANEL may be used to execute some previously defined function that is not normally part of *Neurokit*. In this particular simulation, clicking on `run paradigm` calls up a window containing plots for the six channel currents. Examining these currents before, during, and after a burst should give you further insight into the interplay between the various conductances

during this cycle. Note that we have used the GENESIS convention of plotting inward currents as positive and outward currents as negative. The `Hide Plots` button at the top left of the Channel Currents window may be used to temporarily hide the plots from view while the plotting continues. These additional plots will slow the simulation down considerably. The `Delete Plots` button at the top right of the window will disable plotting of channel currents completely.

Other experiments given in the exercises at the end of the chapter will let you explore the effects of the various ionic conductances on the firing patterns of the model neuron.

7.6 The Traub Model CA3 Pyramidal Cell

We conclude this chapter with a tutorial based on a more complex mammalian neuron model that incorporates channels very similar to the molluscan channels we have described. The associated tutorial simulation uses a *Neurokit* implementation of the hippocampal CA3 region pyramidal cell model of Traub et al. (1991). This single cell model was developed for use in network models, in order to study the synchronized burst firing of CA3 pyramidal cells that occurs during epileptic seizures. It is often the case in computational neuroscience that one begins with an interest in studying the “high level” network behavior of a system, but finds that it is necessary to first model the detailed behavior of the “low level” components in order to reproduce the behavior of the system.

The implementation of this model is described in considerable detail in the original paper, and our treatment is very brief. Thus, it is recommended that this paper be consulted while using the tutorial. In the tutorial, we will explore some of the properties of this model, as well as the ways that these basic conductance types may interact within a multi-compartmental model. The simulation and the details of the model closely follow the description in the paper, except that: (a) Unless otherwise noted, SI units are used throughout. (b) The membrane potential V_m is measured relative to an extracellular potential of zero; thus the nominal resting potential is $-0.06 V$. (c) The synaptically activated channels in compartments 3 and 15 have not been implemented. A more recent 64-compartment model with dendritic branching (Traub, Jeffereys, Miles, Whittington and Tóth 1994) may be found in the cell model archives of the GENESIS Users Group. (See Appendix A.)

This simplified model of the CA3 pyramidal cell has 19 compartments with a soma in the center and two linear chains of compartments to represent the apical dendrites and the basal dendrites. As does the molluscan burster, this cell has fast sodium, delayed rectifier potassium, high threshold calcium, transient potassium, and calcium-activated potassium conductances. As one might expect for neurons in warm-blooded animals, their time constants for activation and inactivation are much smaller than those observed in molluscs. However, the burst is maintained, not by a slow inward B-current, but by an interesting interaction of events in the soma and the dendrites.

Calcium channels turn out to be particularly important in determining the behavior of this cell. Calcium imaging studies (Regehr, Connor and Tank 1989) have shown that, unlike Na channels which are concentrated in the soma, Ca channels are widely spread over the cell membrane, with high concentrations in the distal dendrites where no Na channels are found. Calcium has a high reversal potential, so they can produce action potentials like sodium. However, these high threshold Ca channels become activated at higher voltages than the Na channels, so their conductance needs to be triggered by sodium action potentials. They also have a much larger time constant for inactivation—on the order of 200 msec. The result of this concentration of high threshold calcium channels in the dendrites is that broad action potentials may be triggered in the dendrites by passive propagation of soma action potentials.

Not only do Ca channels have a direct effect on the membrane potential, but they have an indirect effect as well. These slow calcium spikes in the dendrites propagate back to the soma to depolarize it and sustain the burst. As with the molluscan burster, the Ca^{2+} entry during the burst activates potassium channels that conduct outward hyperpolarizing currents, quenching the burst. In this case, the outward current is a sum of two currents. The voltage- and calcium-dependent potassium C-current conductance is similar to that found in molluscs, but has a relatively fast response to changes in the membrane potential at the higher ambient temperatures in mammals. These cells and other mammalian neurons also contain another current that depends only on the much slower variations in Ca^{2+} concentration. This is the AHP (*after-hyperpolarization*) current, which is responsible for the period of hyperpolarization after a burst of action potentials. The transient potassium A-current plays a relatively minor role in this model. It affects the interval and onset of action potentials.

Published data from voltage clamp experiments were used to model the dynamics of these channels and to make reasonable hypotheses about their distribution throughout the cell. Once we have verified that the model can reproduce experimental results, we can use the simulation to understand the ways in which the various channels interact and produce distinctive bursting patterns of action potentials.

7.6.1 Experiments with the Traub Model

Let's begin by trying to reproduce the bursting behavior observed in this cell and described in the paper by Traub et al. Change to the *Scripts/traub91* directory and begin the simulation in the same manner as the *burster* tutorial, starting GENESIS first, and then typing "Neurokit," once GENESIS has begun. As before, use the file menu to load the default cell model. In this case, it will be "CA3." After clicking on run cell in the title bar, you will be ready to try some experiments.

We would like to record from the soma and from a compartment (apical_14) in the apical dendrite which is 0.5 length constants from the soma. These two compartments

are of interest because of their very different concentrations of ion channels. The soma contains the highest concentration of Na channels. Compartment `apical_14` and its adjacent compartments in the apical dendrite contain the highest concentration of Ca channels, but have no Na channels to produce sharp action potentials.

Start by clicking the left button in the soma. A recording electrode should appear and the box labeled `click_site1` should display `"/CA3/soma."` To plant a recording electrode in compartment 14 of the apical dendrite, click the left mouse button about half way to the right along the "fat" dendrite extending from the soma. If the `click_site1` box then shows something other than `"/CA3/apical_14,"` click the middle button in the same place to remove the electrode and try again. With a little practice, you will find it easy to record from any desired part of the cell.

Next, click on `Iclamp` under the **ELECTROPHYSIOLOGY** heading. Underneath, a dialog box labeled `"inject (nanoAmps)"` should appear, with a value of `"0"` in the box. Set the injection value to 0.2 nA . Then click on the soma to plant an injection electrode in the soma. Finally, click on `run` in the **SIMULATION CONTROL PANEL** to start the simulation. Note that most of the buttons and dialog boxes may be used while the simulation is running. For example, you may call up the help window or change the injection current without stopping the simulation. When running long simulations, you may pass the time by consulting the help window or by inspecting the model parameters with the `edit cell` option (described below).

While the simulation is running, you will see the compartments in the cell diagram change color to represent the value of the membrane potential V_m . "Hot" colors represent higher voltages, and "cold" colors represent lower voltages. With some practice, you may use this feature to observe the propagation of action potentials along the dendrites. The `runtime` dialog box shows that the simulation will run for 0.1 seconds of simulation time, and the `current_time` box displays the current simulation time. `clock` shows the default integration time step of `"5e-5"` ($50 \mu\text{sec}$). The `refresh factor` of `"10"` indicates that the graph and the cell diagram will be updated every 10 simulation steps. You may speed up the simulation by increasing this number, at the expense of losing resolution in the plot of action potentials.

The plots below the cell diagram show the membrane potential in the two compartments. The lower one shows a burst of action potentials in the soma that terminates after about 50 msec . If we were to run the simulation longer, we would see another burst in about a second. The curve above, which has been displaced by 100 mV for clarity, shows the membrane potential in the middle of the apical dendrite. Here the spike is very broad and somewhat delayed. There are no Na channels in this region, but the density of Ca channels is high, so we might suspect that we are seeing a Ca action potential on top of whatever soma potential has propagated to this point. This point is 0.5 length constants from the soma. You should verify that the theory of Chapter 5 predicts that the action potentials from the soma will be attenuated by a factor of about 0.6.

We can understand the interaction between these two types of action potentials by paying close attention to the colors in the cell diagram as we step the simulation for short amounts of time. To slow things down a bit, set the `clock` dialog box value to “1e-5” seconds. Then set the `runtime` dialog value to “0.016”, so that the simulation will stop just before the beginning of the burst. Click on the `reset` button in order to reset the simulation time to zero and clear the graph. Then click on `run` again to perform 16 msec of simulation. Now change the `runtime` to only 0.001 seconds, and click on `run` again *without* clicking on `reset`. You may step through the simulation at 1 msec intervals in this manner, watching the propagation of action potentials along the apical dendrite. You should be able to see how the Na action potentials that are generated in the soma propagate to the dendritic compartments where they trigger Ca action potentials. These then propagate back to the soma where they cause the depolarization that maintains the burst and increases the spike frequency during the middle of the burst. Figure 7.3 gives a gray-scale “snapshot” of the situation near the peak in the dendritic calcium spike.

It is also possible to plot other quantities such as channel current or channel conductance on a second graph. In the *burster* tutorial, this graph appeared by default to plot the Ca^{2+} concentration in the soma. Looking at these other variables can help us to understand what mechanisms are responsible for terminating the burst. Click on `Show extra cell window` to bring up a second cell diagram and its associated graph. If you click on the `scale` button in the upper left corner of the second Cell Window, a menu will appear containing a number of dialog boxes. The only two that are relevant at present are `colfield` (containing “Gk”) and `fieldpath` (containing “Ca”). The first of these is the name of the quantity to be plotted on the graph and to be used to determine the color of the compartments. In this case, it is the channel conductance “Gk.” The `fieldpath` contents specify the location of the field to be plotted, i.e., the Ca channel. The compartment is specified in the usual way by planting recording electrodes in the cell diagram. Other channels that you can choose are the Na, K_DR (delayed rectifier), K_AHP (after-hyperpolarization), K_C (C-current), or K_A (A-current) channels. For `colfield` you may choose the channel current (“Ik”), activation variable (“X”), or inactivation variable (“Y”), as well as the conductance (“Gk”). In addition to the channels, each compartment has an element called “Ca_conc” which keeps track of the Ca^{2+} concentration. In order to plot the concentration, you may set `fieldpath` to “Ca_conc” and `colfield` to “Ca.” The `scale` button on the associated graph should be used to set the graph scales to a range consistent with the quantity to be plotted.

For now, let’s go with the default values and plot the Ca channel conductance. Click on `APPLY_AND_VANISH` to put the menu away. Click on the `Recording` button under the `ELECTROPHYSIOLOGY` heading and plant electrodes in the soma and `apical_14` compartment of the second Cell Window. (It is not necessary to apply injection in the second Cell Window, as the injection is being applied in the first.) Set `clock` back to “5e-5,” `runtime` to “0.1,” then click on `reset` and `run`. Note that multiple plots in this second graph window do not have a vertical offset, as is the case with the V_m plots in the first graph. You should

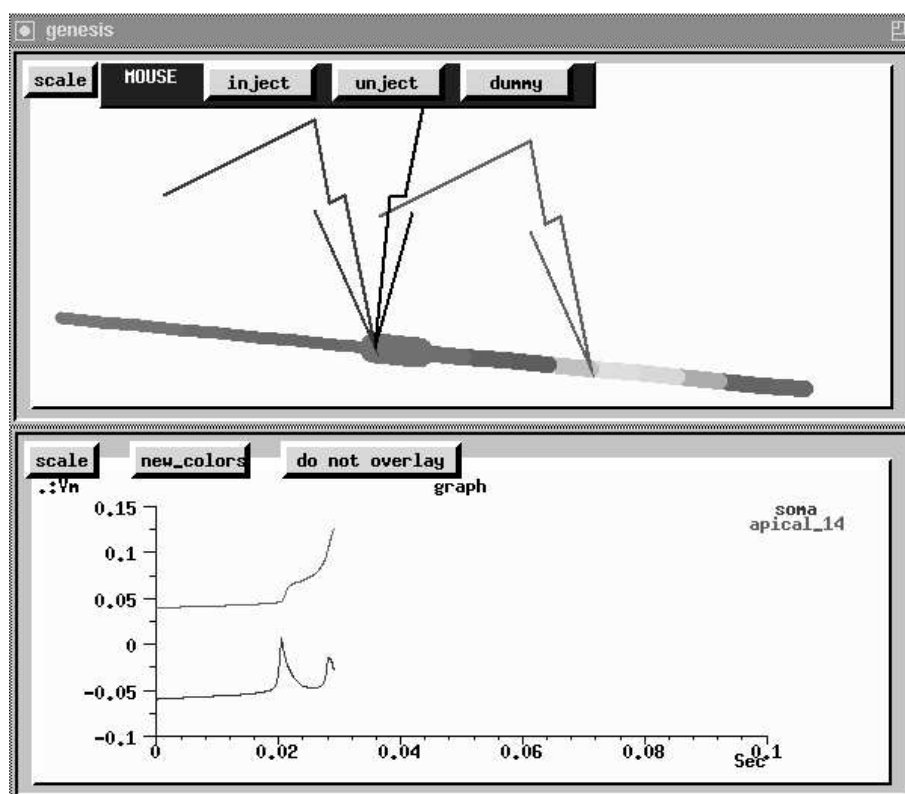


Figure 7.3 The cell diagram for the *traub91* tutorial, showing recording and injection electrodes, and the propagation of action potentials. The plots below show the membrane potential in the soma (lower trace) and in apical dendrite compartment “apical_14” (upper trace).

see a large broad peak in the Ca conductance in the dendrite, corresponding to the voltage peak.

We can make use of the “overlay” feature of the graph in order to compare the timing of the Ca conductance with that of the K_C conductance. In order to overlay the results of a second run using new colors, click on `new_colors` and `do not overlay` at the top of the second (conductance) graph. The label should then change to “overlay,” indicating that the graph will not be cleared on reset. Click on the `scale` button of the second Cell Window, change the `fieldpath` to “K_C,” and then click on `APPLY_AND_VANISH`. Finally, click on `reset`, and then run in the control panel. Notice the position of the peak in the K_C conductance in the apical_14 compartment relative to that of the peak of the Ca conductance. How do these peaks correlate with the shape of the action potential in this compartment?

As these results indicate that Ca and calcium concentration-dependent K conductances

have a lot to do with the bursting behavior, it would be reasonable to repeat the experiment with the Ca channels blocked in order to see if this destroys the bursting behavior. We can use the `edit_cell` selection on the title bar to set the Ca conductance density to zero in every compartment. After you click on this button, a Cell Window with a drawing of the cell should appear in the lower left corner of the screen. Click on the left end of the diagram. The selected compartment will turn red and a labeled diagram of the compartment will appear in the Compartment Window at the upper right of the screen. In this case, the compartment will be the `basal_1` compartment. As it contains no channels, click on the next compartment in the Cell Window. The `basal_2` compartment should now appear in the compartment window, accompanied by icons representing the Ca, `K_AHP`, and `K_C` channels. If you click on the Ca channel icon, the `Selected channel` dialog box will show `“/CA3/basal_2/Ca,”` and the `Conductance` dialog box will show the default conductance density ($50 S/m^2$). Set this value to zero. Now click on the next compartment in the Cell Window. You should now be inspecting the Ca channel of the `basal_3` compartment. (As the Ca channel is the currently selected channel, you will not need to repeat the channel selection.) Set the conductance density to zero and go on to the next compartment. When the Ca conductance density has been set to zero in all the compartments, select `run_cell` from the title bar. (HINT: It is also possible to set various parameters by typing commands to the “genesis” prompt. The command `“setfield /CA3/##/Ca Gbar 0.0”` uses *wildcard* symbols (#) to set the maximum Ca conductance to zero in all the compartments. Chapter 12 explains the use of the GENESIS *setfield* command.) Now click on `reset` and repeat the sequence of steps for plotting the results of applying a $0.2 nA$ injection current to the soma. Can you qualitatively explain the different interval between action potentials in the absence of Ca currents?

7.6.2 Firing Patterns

Experiments have shown that CA3 pyramidal cells have different modes of firing with different amounts of somatic current injection. For small depolarizations, the pattern is one of short bursts separated by a fairly long hyperpolarized interval which decreases as the amount of injection increases. With larger injections, there is a transition to repetitive firing of single action potentials. This can be observed by performing 1.5 second runs with currents of 0.2 , 0.3 and $0.5 nA$ injected to the soma.

After having performed the previous experiment, the fastest way to restore the original conductances and simulation parameters is to quit the simulation and reload the CA3 cell model. Then, proceed as in the first experiment, with a single Cell Window and graph. Record from the soma and the `apical_14` compartment and inject a $0.2 nA$ current to the soma. However, the `runtime` value should be increased to 1.5. The default time scale for the graphs is only 0.1 second, but the scales may be changed while the simulation is running.

Run the simulation and, once the simulation has run past 0.1 second, click on the `scale` button associated with the graph. Change the value in the `xmax` dialog to “1.5” and press the `APPLY_AND_VANISH` button. You may also adjust the value of `xmin` in order to zoom in on a particular pattern of bursts or other features. Note that the existing data will be replotted whenever the scale is changed. Use `overlay` mode and `new colors` to superimpose plots of runs with injections of 0.3 and 0.5 nA. Note the transition between the two firing modes. If you have the time, you might also try injections of 0.1 and 0.8 nA. If you get bored during these long runs, you may amuse yourself by looking at the various options and information available through the `edit_cell`, `edit_compt` and `edit_channel` title bar selections. The simulation will continue to run in the background.

You should note that, with the larger amounts of injection, the cell will settle down to a pattern of regular firing after an initial burst. The larger depolarization provided at these higher injection currents is strong enough to cause somatic action potentials, in spite of the shunting of the membrane by the AHP and other outward currents. However, this shunting is enough to severely attenuate the action potentials by the time they reach the dendrites. Although they cause increases in the Ca conductance, they are unable to provoke full-blown Ca action potentials in the dendrites. The result is that enough Ca enters the cell to maintain the dendritic shunt from the calcium-activated conductances, but not enough to stop the production of action potentials in the soma. Exercise 8 asks you to further explore the details of this firing mode and of a third mode that is predicted by the model.

7.7 Exercises

1. Some explanations or models of bursting in the *Aplysia* R15 neuron ignore the high threshold Ca current. Explore the effects of eliminating this current by setting its maximum conductance to zero. You may do this by selecting `edit_cell` from the top menu bar. Click on the soma in the lower left window and then click on the icon for the Ca channel in the upper right window. Change the `Conductance` dialog value from 65.2 to 0, and hit “Return.” Click on `run_cell` in the title bar. Finally, click on `reset` and `run`. Explain the reasons for the differences that you see.
2. The *Aplysia* L11 cell is a repetitively discharging pacemaker (“beater”) instead of a “burster.” Gorman and Hermann (1982) have estimated that in the R15 cell, the conductance density for the B-current channels is 6 times greater, that of the high threshold Ca channels is 8 times greater, and that of the K_C channels is 23 times greater than in the L11. Use `edit_cell`, as described in the previous exercise, to transform the model cell to a “beater.”
3. When sodium channels are blocked with TTX, a slow oscillation in the R15 membrane potential is seen. Set the Na conductance to zero and compare the period of the

resulting slow oscillation to that of the bursts when the Na conductance is present. How does it compare to the period of the bursts in Exercise 1? Can you explain any differences? (For these measurements, use the `scale` button on the graphs to increase the time scale to 80 seconds and run the simulation for 80 seconds.)

4. Examine the effect of the A-current by performing one of these two experiments on the molluscan burster model.
 - (a) Use the default parameters for producing bursts and set the time scale for the V_m plot so that you can observe the second burst in detail. Notice that the firing rate increases at the beginning of the burst and then decreases at the end, approximately following the pattern of the “slow oscillation”. After studying the results, set the channel conductance for the A-current to zero and repeat the experiment. What differences do you see? Also compare the shape of the action potentials with and without the A-current. Explain these results in terms of what you know about the properties of the A-current. It will be useful to refer to the A-current activation/inactivation curves and their time constants.
 - (b) Alternatively, examine the effects of the A-current in the absence of the Ca-, B- and C-currents by setting their maximum channel conductances to zero. This will leave only the Na-, K- and A-currents present. Without the inward B-current, you will need some current injection in order to produce firing, so set the injection current to 1 nA. (You may do this by clicking on `Iclamp`, planting an injection electrode in the soma in the left Cell Window, and entering the current in the `inject` dialog box.) Estimate the firing rate and repeat for 2, 3, 4 and 5 nA injections. Then remove the A-current and estimate the firing rate for these injection currents. As in part (a), explain the differences in response and in the shape of the action potentials.
5. In Exercise 8 of Chapter 4, we used the *Squid* tutorial to examine the phenomenon of “anode break” (posthyperpolarization rebound). Insert a current injection electrode into the molluscan cell as described above, but leave the injection current set to zero. Run the simulation for about 15 seconds, so that it ends during the interburst interval. Now set the injection current to -5 nA and the run time to 5 seconds. After running for 5 seconds, restore the injection current to zero and run for another 15 seconds. Explain the reasons for the differences between this experiment and the case with “squid-like” Hodgkin-Huxley channels. (Hint: it may be useful to observe the sodium inactivation variable during the course of the experiment. You may plot it, rather than the Ca^{2+} concentration, by clicking on the `scale` button in the right-hand Cell Window (labeled “molluscxout2”). When the scale menu comes up, change the `colfield` dialog box entry to “Y” and the `fieldpath` to “Na.” Now use the `scale` button on the graph below to set `ymax` to 1.)

6. In Sec. 7.3, we mentioned that some molluscan pacemakers have a “shoulder” on the downward slope of their action potentials (Aldrich, Getting and Thompson 1979b). This is not seen in recordings from *Aplysia* R15 cells, nor in our simulation. Examine the effect of the Ca conductance on the width and shape of the action potentials in the molluscan burster model. It will be best to “zoom in” on the second burst by adjusting the values of `xmin` and `xmax` in the `scale` menu for the graph that plots V_m . Although it will slow the simulation down somewhat, you may also wish to set the `refresh_factor` dialog value to a lower value in order to increase the resolution of the plot.

After using `edit cell` to remove the Ca conductance and noting whether or not this has any significant effect on the action potentials, restore the conductance and try shifting the threshold for Ca activation to lower voltages. This may be done with the `edit channel` selection. Follow the procedure given in Sec. 7.5 for examining the Ca channel activation gate. Then apply a negative offset to the voltage axis for the gate by entering it in the `ox` dialog box. You might begin with a value of “-0.010” in order to shift the activation curve down by 10 mV. Clicking on the `m_inf` button will apply this offset to the steady-state activation curve (m_∞ , which we have called X_∞). Each time you click on `m_inf`, the offset will be applied to shift the curve down by an additional 10 mV. Examine the second burst with various thresholds for Ca activation. Describe and explain your results.

7. In an earlier experiment with the CA3 pyramidal cell model, we studied the behavior of the Ca and K_C conductances during a burst. In a similar manner, look at the K_AHP conductance during the interval between bursts. What happens when this conductance is set to zero in all compartments? What happens when the K_AHP conductances are restored and the K_C conductances are removed instead? Use these results to explain why, unlike the molluscan bursters, the CA3 pyramidal cell requires both of these calcium-activated potassium currents for burst firing.
8. The paper by Traub et al. (1991) describes a third firing mode which is predicted by the pyramidal cell model when the cell is subject to large amounts of depolarizing dendritic stimulation. In the simulation, this can be provided by injecting a moderately large current into the distal dendrite region. Try injecting 1.5 nA into the `apical_15` compartment and note the firing patterns. In addition to monitoring both V_m and the Ca conductance, do some runs with plots of the K_AHP conductance for this situation and for the low and high current injections to the soma which were described earlier. Use these results to give a detailed explanation of how the three different firing patterns arise.
9. Try some voltage clamp experiments on the CA3 pyramidal cell model by selecting `Vclamp` from the `run cell` menu. (Before leaving `Iclamp` mode, be sure to use

the middle mouse button to remove any current injection electrodes!) For example, clamp the membrane potential to the nominal resting potential, -0.060 V. Look at the steady-state values of each of the ion channel currents in the soma and other selected compartments. What can one learn from this?

10. Traub et al. (1991) describe two other cell models: an acutely isolated cell (soma plus the two adjacent compartments) and a CA1 region cell model. To load the former model, select the `file` menu from the title bar after quitting and starting a new session with *Neurokit*. Then enter `/acute` in the `Cell for IO` dialog box and `acute.p` in the `source file name` dialog box before clicking on `Load from file`. As before, select `run cell` from the title bar. When the cell diagram appears, click on `Recording` and plant some electrodes. If the cell diagram is not properly centered, you may move it to the left or the right by hitting `Ctrl-H` or `Ctrl-L` while the cursor is in the `Cell Window`. Switch to `Iclamp` mode and try some of the experiments described in the paper. Try to reproduce and explain the results shown in Fig. 4 of their paper.

For the CA1 model, the entries are `/CA1` and `CA1.p`. Note that the different distribution of channels yields different firing patterns from those observed in the CA3 model. Why is there no burst firing when injection is provided to the soma?